Phys. Lett. B 853 (2024) 138688

Contents lists available at ScienceDirect

Physics Letters B

journal homepage: www.elsevier.com/locate/physletb

Letter

Echoes of massless scalar field induced from hairy Schwarzschild black hole

Zhen-Hao Yang, Cheng Xu, Xiao-Mei Kuang *, Bin Wang, Rui-Hong Yue

Center for Gravitation and Cosmology, College of Physical Science and Technology, Yangzhou University, Yangzhou, 225009, China

ARTICLE INFO

Editor: N. Lambert

ABSTRACT

A hairy Schwarzschild black hole describes the deformation of Schwarzschild black hole with an exponent correction due to the introducing of additional sources. Inspired by the novel feature that the hairy Schwarzschild black hole can have double photon spheres for certain parameters space, in this paper we study the echo signals of a massless scalar field from this hairy Schwarzschild black hole by calculating its time evolution. We mainly analyze how the hairy parameters and scalar field's angular momentum affect the echo waveform of the perturbing scalar field. Additionally, we roughly evaluate the time delay of echoes. We find that the hairy parameters have significant influences on the echo signals.

Contents

1. Introduction

The astrophysical observation on the gravitational wave (GW) [1–3] released from the binary black holes opens a new window for us to explore our Universe. In general, the binary massive objects merging events can be divided into three stages [4–6], i.e., the inspiral stage, the merger stage, and the ringdown stage. Each stage needs proper method to study their characterized features. The post-Newtonian approximation is usually used to describe the inspiral stage [7] and numerical general relativity should be employed to simulate the merger stage [8]. While in the ringdown phase, since the spacetime approaches to be stationary so that one can use the quasinormal modes (QNMs) to reflect the properties, especially when the final state is a black hole [5,9]. However, it was addressed in [5] that QNMs are closely related to the light rings of massive objects, which are not necessarily black holes. Therefore, only by the features of QNMs, it is unconvincing to distinguish black holes from Exotic Compact Objects (ECOs), whose external spacetime has the same geometry as a black hole [9].

Another potential probe is the GW echo [10–12], which is the GW signals reflected from the near-horizon region of the final massive object formed during the merger process. The authors of [13] emphasized that the GW echo could be a good probe of even Planck-scale structures near

* Corresponding author
E-mail address: xmeikuang@yzu.edu.cn (X.-M. Kuang).

https://doi.org/10.1016/j.physletb.2024.138688
Received 5 March 2024; Received in revised form 9 April 2024; Accepted 29 April 2024
Available online 6 May 2024

the horizon [10] since the lag of echoes behind the main wave corresponds to the exponentially small distance between the ECO surface and the location of the horizon. So far, though we still have no statistically significant evidence for the existence of echoic GW data [14–20], the echo signal would be a promising candidate for probing physics beyond GR. In particular, it was suggested in [10,21] that echo signal could be a potential probe to distinguish the source of gravitational waves, saying to tell whether the GW is from a black hole or not. Recent researches showed that echo signals could arise in wormholes [22–26] and diverse sources including compact objects [27], quark stars [28], braneworld black holes [29], and even from a singularity [30], but initially it was found hard to obtain echo signals from the black hole. Nevertheless, more recently, echoes from black hole modified from those in Einstein theory are extensively explored in [31–38]. Those studies indicate that the echoes in black holes seem not to be rare so as to deserve wide researches. In particular, it was believed that the echoes could only occur in the spacetime which has effective potential with double or more peaks.

On the other hand, a hairy Schwarzschild black hole, which includes an exponent term modified from the Schwarzschild black hole in GR, was recently obtained by using the gravitational decoupling (GD) approach [39,40]. The hairy Schwarzschild black hole was designed for describing the deformations of known solutions of GR due to the inclusion of additional sources. How the metric is solved from the GD approach will be briefly reviewed in the next section. The hairy Schwarzschild black hole and its rotating counterpart have attracted plenty of interests, which are extensively studied: the thermodynamics [41], quasinormal modes and (in)stability [42–44], strong gravitational lensing and black hole shadow [45–48], Lense-Thirring effect and quasi-periodic oscillations [49,50], and gravitational waves from extreme mass ratio inspirals [51] and so on. All these results promote the potential test of the no-hair theorem and provide powerful probes of alternative theories of gravity with additional fields in this scenario.

In particular, the hairy Schwarzschild black hole was found to have two photon spheres outside the event horizon by analyzing the effective potential of the radial null geodesic motion [52]. Then it was addressed in [47] by some of us that the double photon spheres resulting from the additional hair have significant influences on the optical appearance of the black holes illuminated by various accretions. According to geometry-optical approximation [53], we can expect that due to the existence of double photon spheres, the perturbed fields of this black hole could have effective potential with two peaks. Thus, as a first attempt, the aim of this paper is to study the waveform of massless scalar field which is a probe around the hairy Schwarzschild black hole. We will examine that the waveform will be reflected between the two potential barriers and echo signals can be observed, differentiating from that in Schwarzschild black hole. We will focus on the effects of the deviation parameter and hairy charge on the waveform and echo timescale, respectively. It is worthwhile to point out that since the hairy black hole in this scenario has great generality because there are no certain matter fields in the GD approach, so this hairy metric with an exponent term modified from the Schwarzschild black hole in GR allows us to study the echoes introduced by arbitrary type of hair (e.g. scalar hair, tensor hair, fluid-like dark matter, and so on).

The remaining of this paper is organized as follows. In section 2, we will review the hairy Schwarzschild black hole constructed in the GD approach, and analyze the peak of the effective potential of the massless perturbing scalar field in this background. In section 3, we show the waveform of the scalar field in time domain, and analyze the effects of hairy parameters on the echoes and its time delay. Section 4 contributes to our conclusion and discussion.

2. The preliminary setup

In this section, after briefly reviewing the construction of the hairy Schwarzschild black hole from the GD approach [39], we will analyze the effective potential of massless scalar field in the hairy Schwarzschild black hole.

2.1. Review of the hairy Schwarzschild black hole

The interaction between black hole spacetime and matters could introduce an additional charge, making the final black hole carry hairs and hairy black holes may form, which will avoid the no-hair theorem in classical GR [54]. Recently, a spherically symmetric metric with hair was obtained by using the so-called GD approach [39]. In this scenario, the Einstein equation is written as

$$G_{\mu\nu} \equiv R_{\mu\nu} - \frac{1}{2}Rg_{\mu\nu} = 8\pi\tilde{T}_{\mu\nu}, \tag{1}$$

where the total energy momentum tensor $\tilde{T}_{\mu\nu} = T_{\mu\nu} + \vartheta_{\mu\nu}$ has two parts: $T_{\mu\nu}$ the energy momentum tensor associated with a known solution of GR and $\vartheta_{\mu\nu}$ introduced by new matter fields or a new gravitational sector. The Bianchi identity requires that $\nabla^{\mu}\tilde{T}_{\mu\nu} = 0$. The main aspect of GD approach, originally given in [55], is that $\vartheta_{\mu\nu}$ can be decoupled from $T_{\mu\nu}$ [39,40]. In order to give the construction of a deformed solution with the GD approach, we will list the main technical points, and then demonstrate that under the decoupling assumption, one could indeed decouple the equations of motion for the two sectors. Firstly, the spherically symmetric and static solution $g_{\mu\nu}$ to (1) can be written as

$$ds^2 = -e^{\nu(r)}dt^2 + e^{\lambda(r)}dr^2 + r^2(d\theta^2 + \sin^2\theta d\phi^2), \tag{2}$$

from which we can express the Einstein tensor $G_{\mu}^{\ \nu}(\nu(r), \lambda(r))$. Secondly, the above solution (2) is assumed to be generated from the seed metric with only the source $T_{\mu\nu}$ but $\vartheta_{\mu\nu} = 0$,

$$ds^2 = -e^{\xi(r)}dt^2 + e^{\mu(r)}dr^2 + r^2(d\theta^2 + \sin^2\theta d\phi^2). \tag{3}$$

Then, the deformation of the seed metric

$$\xi(r) \to \nu(r) = \xi(r) + \alpha\ k(r), \qquad e^{-\mu(r)} \to e^{-\lambda(r)} = e^{-\mu(r)} + \alpha\ h(r), \tag{4}$$

completely attributes to the introduction of $\vartheta_{\mu\nu}$, and the parameter α keeps track of the deformations. Subsequently, the Einstein equation (1) is split into the standard Einstein equation $G_{\mu}^{\ \nu}(\xi(r), \mu(r)) = 8\pi T_{\mu}^{\ \nu}$ and an additional one $\alpha\ \mathcal{G}_{\mu}^{\ \nu}(\xi(r), \mu(r); k(r), h(r)) = 8\pi\vartheta_{\mu}^{\ \nu}$, from which it is obvious that $\vartheta_{\mu\nu}$ vanishes once $\alpha = 0$ as expected. In addition, it is easy to obtain that under the transformation (4), the Einstein tensor transfer as

$$G_{\mu}^{\ \nu}(\xi(r), \mu(r)) \to G_{\mu}^{\ \nu}(\nu(r), \lambda(r)) = G_{\mu}^{\ \nu}(\xi(r), \mu(r)) + \alpha\ \mathcal{G}_{\mu}^{\ \nu}(\nu(r), \lambda(r)), \tag{5}$$

which is a linear decomposition of the Einstein tensor. The similarity between the linear decomposition of the Einstein tensor and the two sources added linearly in the r.h.s of (1) is the important aspect that makes the GD approach work in seeking the analytical solution to the equations of motion.

The simplest case is to consider the seed metric (3) as the Schwarzschild one with the vacuum $T_{\mu\nu} = 0$. Further treating the additional source as the anisotropic fluid which satisfies the strong energy condition, the authors of [39,40] solve out the Einstein equation and obtain the hairy solution deformed from the Schwarzschild metric. Since their calculations are straightforward, here we will omit their steps and directly give the hairy Schwarzschild black hole with the metric

$$ds^2 = -f(r)dt^2 + \frac{dr^2}{f(r)} + r^2(d\theta^2 + \sin^2\theta d\phi^2)$$
$$\text{with} \quad f(r) = 1 - \frac{2M}{r} + \alpha e^{-r/(M - l_o/2)}. \tag{6}$$

It is obvious that this metric describes the deformation of the Schwarzschild black hole solution due to the introduction of additional sources, which can be dark matter, scalar fields, tensor fields, etc. The technical steps in the GD approach to construct the deformed solutions are good, but the specific background theory, which can give the energy momentum tensor $\vartheta_{\mu\nu}$ in the assumption, remains unclear. In [39], the authors briefly discussed the possible specific theories which still call for further investigations. Even so, considerable theoretical and observable related properties of this deformed black hole have been explored, see for examples [41–51] and references therein. It is believed that more complete understanding on the phenomena of this deformed black hole could further help us to build its background theories. In this paper, instead of clarifying its corresponding background theory, we shall discuss the perturbed scalar field propagating around the hairy black hole. In the metric (6), M denotes the black hole mass, and α is the deformation parameter. $l_o = \alpha l$ with l a parameter, is the charge of primary hair which should satisfy $l_o \leq 2M$ to make the deformed black hole be asymptotically flat. The event horizon of this hairy Schwarzschild black hole can be determined by numerically solving the following equation

$$f(r)\,|_{r=r_h} = 0 \Rightarrow r_h + \alpha r_h e^{-r_h/(M-l_o/2)} = 2M \tag{7}$$

which has a unique positive root, indicating the event horizon. It is noted that the prescription of strong energy condition requires $r_h \geq 2M - l_o$ [39].

2.2. The effective potential of massless scalar field

We then consider that the massless scalar field $\Phi(t,r,\theta,\phi)$ propagates in the hairy Schwarzschild black hole, which is determined by the Klein-Gordon (KG) equation

$$\Box\Phi = \frac{1}{\sqrt{-g}}\partial_\mu(g^{\mu\nu}\sqrt{-g}\partial_\nu\Phi) = 0, \tag{8}$$

where $\Box$ is the Laplace operator and g is the determinant of the black hole metric (6). To proceed, we decompose the scalar field into

$$\Phi(t,r,\theta,\phi) = \sum_{\ell m}\frac{\psi(r)}{r}Y_{\ell m}(\theta,\phi) \tag{9}$$

where $Y_{\ell m}(\theta,\phi)$ is the spherical harmonic function with angular momentum ℓ and azimuthal number m. Then, under the tortoise radial coordinate r_* defined by $dr_* = dr/f$, the KG equation (8) is reduced to the Schrödinger-like equation

$$\frac{\partial^2\psi}{\partial r_*^2} - \frac{\partial^2\psi}{\partial t^2} - V(r)\psi = 0, \tag{10}$$

in which the effective potential is

$$V(r) = f(r)\left(\frac{\ell(\ell+1)}{r^2} + \frac{f'(r)}{r}\right), \tag{11}$$

and the azimuthal number m does not appear due to the spherical symmetry of the spacetime. It is obvious that the evolution of the scalar field will strongly depend on the profile of the effective potential. By tuning the parameters, we find that the potential (11) can have one peak or two peaks depending on the values of the parameters. To check the influence of the hairy parameters, we fix $M = 5$ and $\ell = 2$ and scan the space $(\alpha, l_o/M)$ of the black hole parameters. We find a region of $(\alpha, l_o/M)$ space in which the effective potential (11) has two peaks, zoomed in Fig. 1. We see that for a fixed deviation parameter α, only a small region of the hairy parameter l_o/M can give double peaks of V if exist, and vice versa. Since the wave can be reflected between the peaks of the effective potential, we expect that for the hairy Schwarzschild black hole with parameters giving effective potential with double peaks, one can observe the echoes of the massless scalar field, differentiating from the cases with single peak including the Schwarzschild case. Thus, we then check how the waveform of the scalar field would be affected by the black hole parameters α and l_o, and also the angular momentum ℓ. We shall fix $M = 5$ for simplification.

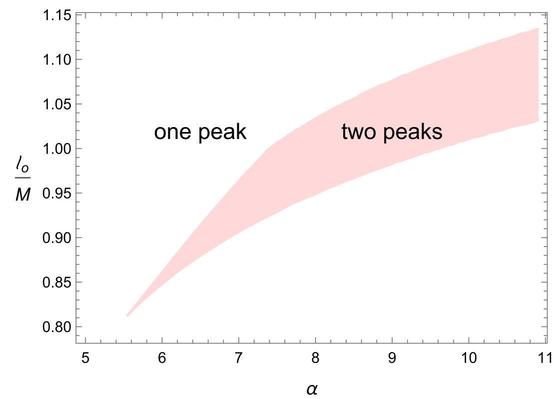

Fig. 1. The parameter region in $(\alpha, l_o/M)$ plane that the potential has one peak (white region) and two peaks (pink region). Here we set $M = 5$ and $\ell = 2$.

3. Waveform in time domain

3.1. Numerical method

To solve the Schrödinger-like equation (10), we have to deal with the time-dependent evolution problem. A convenient way is to adopt the finite difference method [56] to numerically integrate the equation at the time coordinate and fix the space configuration with a Gaussian wave as an initial value. To proceed, we discretize the radial coordinate via

$$\frac{dr(r_*)}{dr_*} = f(r(r*)) \Rightarrow \frac{r(r_{*j}+\Delta r_*) - r(r_{*j})}{\Delta r_*} = \frac{r_{j+1}-r_j}{\Delta r_*} = f(r_j)$$
$$\Rightarrow r_{j+1} = r_j + \Delta r_* f(r_j). \tag{12}$$

So, a list of $\{r_j\}$ is generated if one chooses the seed $r_0 = r_{horizon} + \epsilon$ with a given grid interval Δr_*. We further discretize the effective potential into $V(r(r_*)) = V(j\Delta r_*) \equiv V_j$ and the field into $\psi(r,t) = \psi(j\Delta r_*, i\Delta t) \equiv \psi_{j,i}$. Subsequently, the wave-like equation (10) becomes a discretized equation

$$-\frac{\psi_{j,i+1} - 2\psi_{j,i} + \psi_{j,i-1}}{\Delta t^2} + \frac{\psi_{j+1,i} - 2\psi_{j,i} + \psi_{j-1,i}}{\Delta r_*^2} - V_j\psi_{j,i}$$
$$+ \mathcal{O}(\Delta t^2) + \mathcal{O}(\Delta r_*^2) = 0. \tag{13}$$

Then, we can solve out $\psi_{j,i+1}$ as

$$\psi_{j,i+1} = \frac{\Delta t^2}{\Delta r_*^2}\psi_{j+1,i} + \left(2 - 2\frac{\Delta t^2}{\Delta r_*^2} - \Delta t^2 V_j\right)\psi_{j,i} + \psi_{j-1,i} - \psi_{j,i-1}, \tag{14}$$

which is an iterative equation and can be solved once we set a Gaussian wave packet $\psi_{j,0}$ as the initial perturbation. In our calculations, we shall set $\epsilon = 10^{-15}$, $\Delta r_* = 0.15$, $\Delta t = 0.075$, $\psi_{j,0} = \exp[-\frac{(r_j-a)^2}{b}]$ and $\psi_{j,i<0} = 0$.

3.2. Echoes waveform

We shall present the waveforms of the scalar field in time domain at $r = a$ for some selected parameters in this section.

We first focus on the effect of the deviation parameter α on the wave profile of $\ell = 2$ scalar field mode. Thus, we fix $l_o/M = 1.02$ and choose $\alpha = 7.312, 7.812, 8.312, 9.312, 10.812$, respectively. The time evolution of the perturbed massless scalar field is shown in the left panel of Fig. 2. For $\alpha = 7.812$ and 8.312, we can explicitly see the echoes of the scalar field while only ringdown waveform can be seen for other selected values of α. This phenomenon can be understood from the profile of the effective potential, shown in the right panel of Fig. 2. The effective potential for $\alpha = 7.812$ and 8.312 has two obvious peaks, so the scalar wave can be reflected between the peaks which gives echo signals for

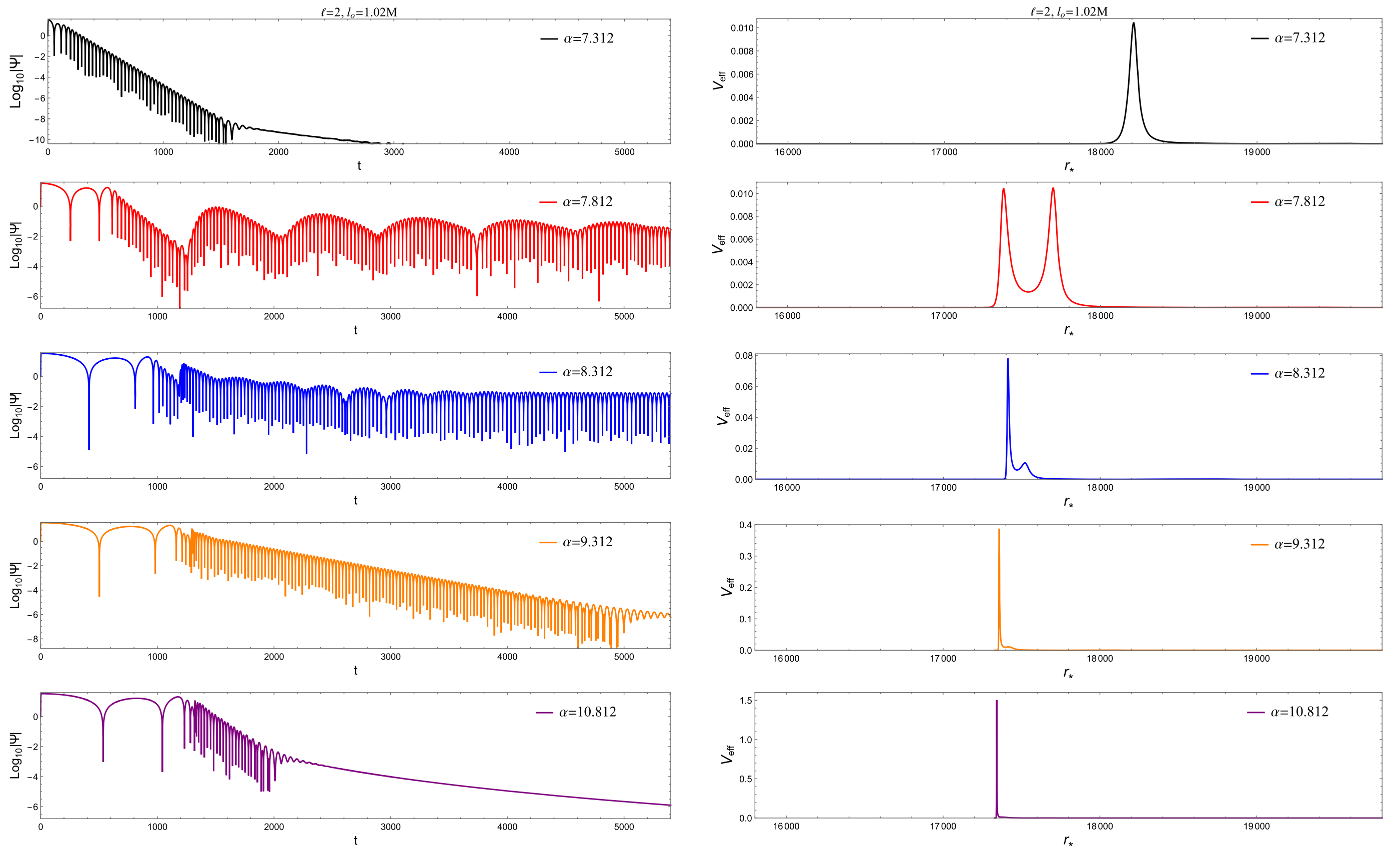

Fig. 2. The waveform (left panel) and effective potential (right panel) for the $\ell = 2$ scalar field mode with some selected α. Here we fix $M = 5$ and $l_o = 1.02M$. Additionally, we set $a = 930$ and $b = 2$ in the initial Gaussian wave.

the far observers. It is noted that though $\alpha = 9.312$ falls into the double peaks region in Fig. 1 such that double peaks appear, but we cannot see the echo signal. This is because comparing to the inner peak, the outer peak is low enough to be ignored and it is difficult for the wave to propagate backforward. Additionally, the selected $\alpha = 7.312$ and 10.812 fall into the single-peak region of Fig. 1, so no echo signal can be observed which is similar to that occurs in Schwarzschild black hole.

In Fig. 3, we show the time evolution and the effective potential of the $\ell = 2$ scalar field mode for the selected $l_o/M = 0.93, 0.96, 0.99, 1.02, 1.05$ with fixed $\alpha = 7.812$. It is obvious that for the cases with effective potential having a broader width of peaks, the echo signals are more obvious. Small or Large enough l_o/M corresponds to the effective potential with single peak, so one can only see the ring-down wave without echoes. Now let us compare Fig. 2 and Fig. 3 to analyze the effects of model parameters α and l_o. In the parameter spaces with double peaks, when α (l_o/M) increases (decreases), the inner peak of the effective potential becomes higher and narrower while the outer peak changes differently, which makes the echo signal weaker and weaker. It implies that the parameters α and l_o/M have competitive effects on the properties of echoes, and one can also see the time delay of echo that we will study in the next subsection. These competitive effects between α and l_o/M were also found in other observables, such as black hole shadows [47].

Then, we will check the effect of the angular momentum ℓ on the echoes of massless scalar field. To this end, we fix $\alpha = 7.812$ and $l_o/M = 1.02$, and present the waveform in time domain and the effective potential for $\ell = 0, 1, 2, 3$ in Fig. 4. The effective potential always has two peaks, and echo waves can be observed for all the selected parameters. As ℓ increases, both peaks become higher while the width between them changes slightly. Thus, the echo signal appears almost at the same time for each ℓ, but for the mode with larger ℓ it can last longer.

3.3. Time delay of echoes

Since the echo signal in our scenario stems from the trapped wave between the double peaks of the effective potential, so the time delay between two consecutive echoes can be roughly evaluated by the time that the light spends for a round trip between the peaks [21]. Thus, we roughly calculate the time delay of echo in our model as

$$\delta t \sim 2 \int_{r_1}^{r_2} \frac{dr}{f(r)}, \tag{15}$$

where r_1 and r_2 are the locations of the two peaks of the effective potential respectively, and $f(r)$ is the redshift function in the metric (6). It is obvious that the hairy parameters will affect the time delay of echoes. According to (15), we numerically evaluate δt in the $(\alpha, l_o/M)$ space in which the effective potential has two peaks (please see Fig. 1) and the density plot of our results is shown in Fig. 5. It is shown that the time delay of echo is shorter (longer) as the increasing of α (l_o/M), which is consistent with what we observed from the waveform in the previous subsection. It is noted that our calculation is based on the fact that the echoes can be observed once the potential with double peaks appears. Though our consideration is ideal and the echo signal indeed depends on a more complex environment, these results in fact give basic physics about how the hairy parameters affect the time delay of the echo signal, which is enough for our purpose.

4. Conclusion

The hairy Schwarzschild black hole constructed with gravitational decoupling proposal describes the deformation of the standard Schwarzschild black hole due to the introducing of additional sources (scalar hair, tensor hair, fluid-like dark matter, etc). It was found

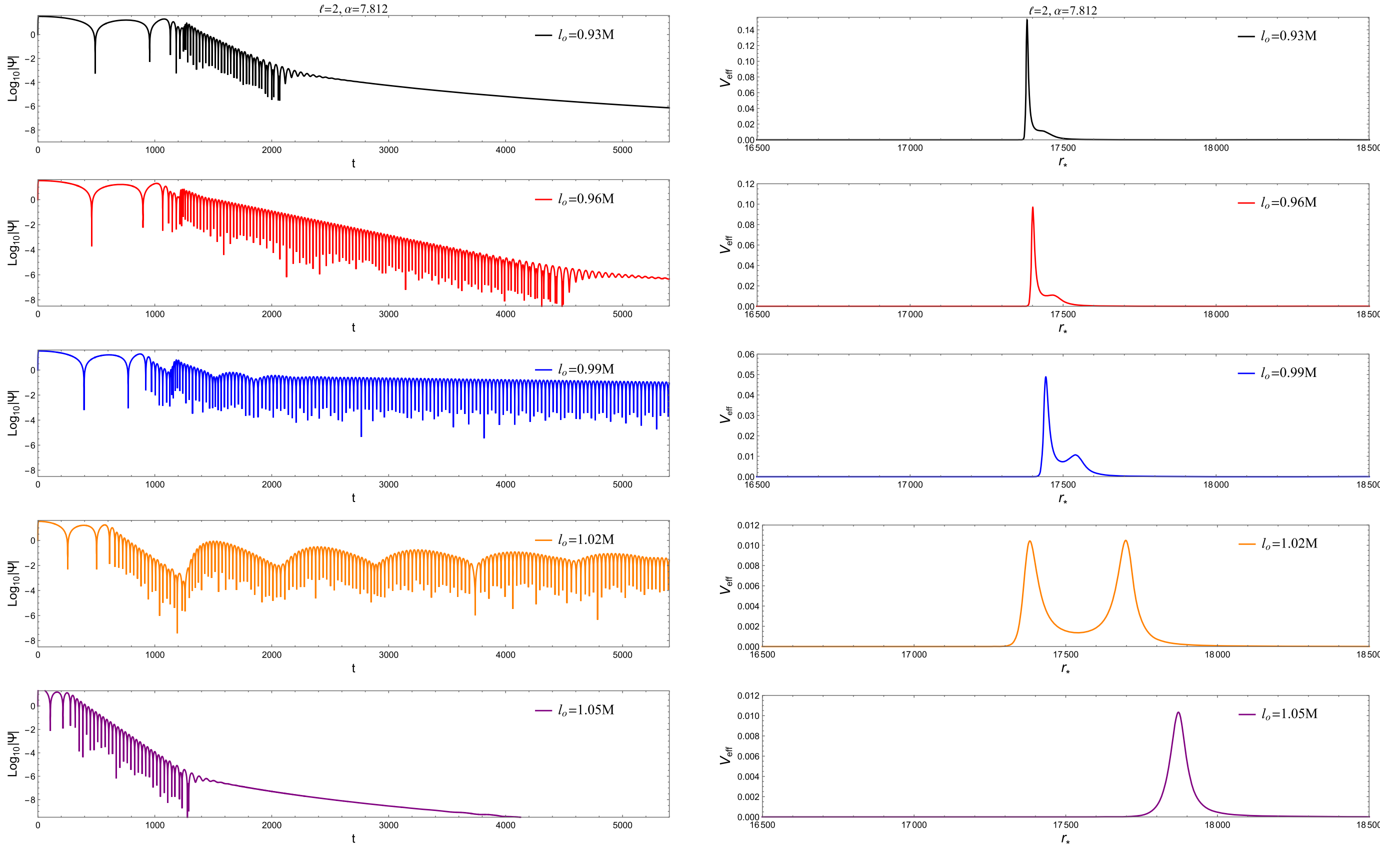

Fig. 3. The waveform (left panel) and effective potential (right panel) for the $\ell = 2$ scalar field mode with some selected l_o/M. Here we fix $M = 5$ and $\alpha = 7.812$. Additionally, we set $a = 654$ and $b = 2$ in the initial Gaussian wave.

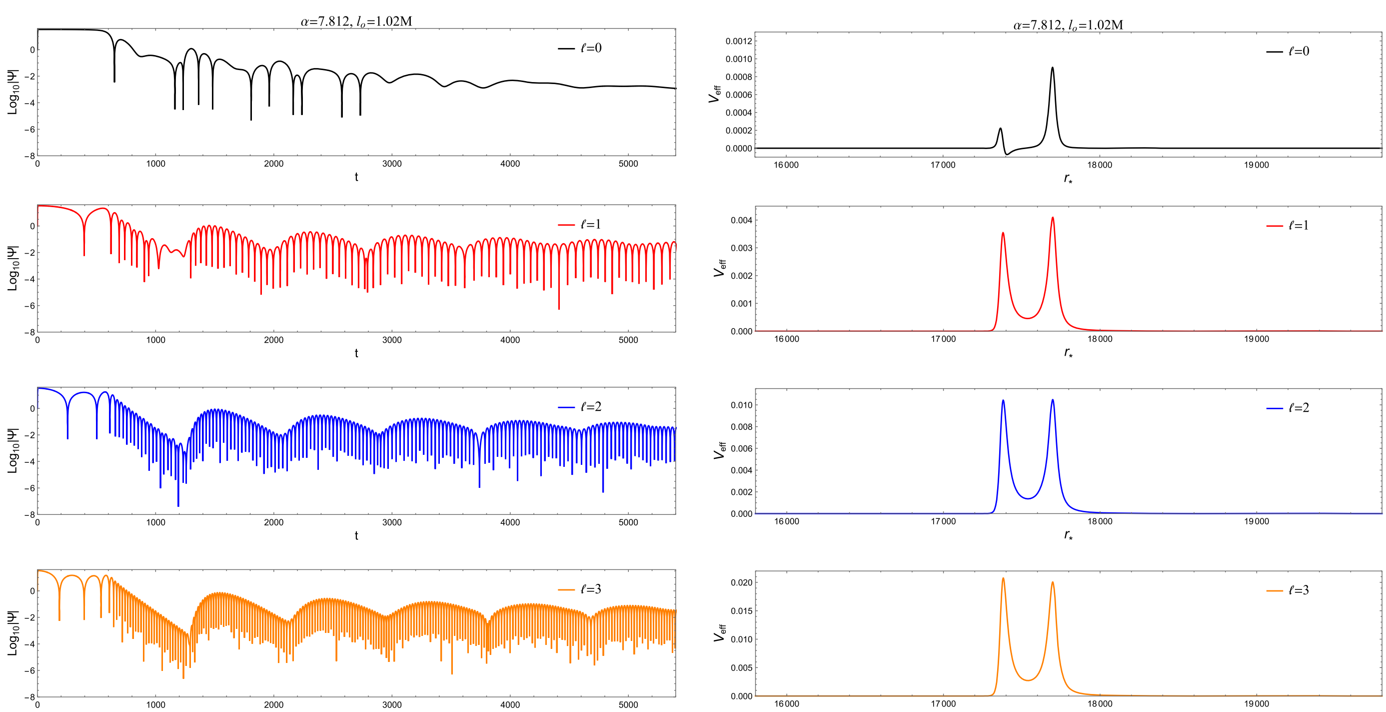

Fig. 4. The waveform (left panel) and effective potential (right panel) for the massless scalar field mode with different angular momentum ℓ. Here we fix $M = 5$, $\alpha = 7.812$ and $l_0 = 1.02M$. Additionally, we set $a = 570$ and $b = 2$ in the initial Gaussian wave.

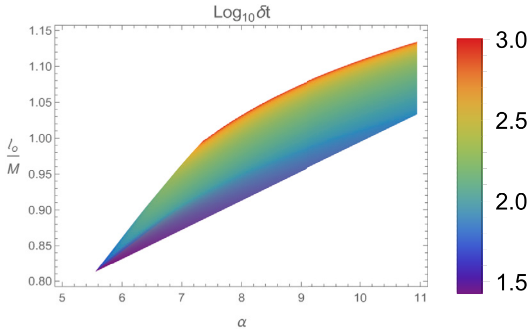

Fig. 5. Time delay of echoes with $M = 5$ and $\ell = 2$.

in [52] that different from the Schwarzschild black hole, the hairy Schwarzschild black hole can have double photon spheres for suitable parameters $(\alpha, l_o/M)$. Inspired by the recent study that the existence of echo signal from the central object was closely related to having multiple photon spheres, in this paper, we studied the echoes of a massless scalar field released from the hairy Schwarzschild black hole.

We first figure out the parameter space $(\alpha, l_o/M)$ in which the effective potential of the scalar field has double peaks. Then by studying the time involution of the scalar field, we analyzed the effects of model parameters on the echo waveforms. For the parameters with deeper and wider well between the two barriers of potential, the echo signal is more obvious. This is because the deeper and wider well between two peaks makes the wave be reflected more easily forward and backward to produce echo signals. In the parameter space $(\alpha, l_o/M)$ with two peaks, we found that decreasing (increasing) α (l_o/M) corresponds to a deeper and wider well in the effective potential, such that the echo signal is stronger and lasts longer. Finally, we roughly evaluated the time delay of echoes using the time that the light takes for a round trip between the peaks, which increases as α (l_o/M) decreases (increases), and matches what we observe from the echo waveforms.

The echo signal is highly expected to be extracted from the gravitational wave events, which could further help us to understand the gravity structure of the wave source. Though here our study is focused on the echoes of perturbed scalar field as an attempt, we hope that our study could inspire more studies related to the echoes from hairy black holes. Thus, one interesting direction is to extend our study into the gravitational wave echoes, and then analyze the prospects of observing the current hairy black hole from echo signals.

Declaration of competing interest

The authors declare that they have no known competing financial interests or personal relationships that could have appeared to influence the work reported in this paper.

Data availability

No data was used for the research described in the article.

Acknowledgements

This work is partly supported by the Natural Science Foundation of China under Grants No. 12375054 and Natural Science Foundation of Jiangsu Province under Grant No. BK20211601.

References

[1] B.P. Abbott, et al., LIGO Scientific, Virgo, Phys. Rev. Lett. 116 (2016) 061102, arXiv:1602.03837.
[2] B.P. Abbott, et al., LIGO Scientific, Virgo, Phys. Rev. X 9 (2019) 031040, arXiv:1811.12907.
[3] B.P. Abbott, et al., LIGO Scientific, Virgo, Astrophys. J. Lett. 892 (2020) L3, arXiv:2001.01761.
[4] B.P. Abbott, et al., LIGO Scientific, Virgo, Phys. Rev. Lett. 116 (2016) 221101; Phys. Rev. Lett. 121 (2018) 129902 (Erratum), arXiv:1602.03841.
[5] V. Cardoso, E. Franzin, P. Pani, Phys. Rev. Lett. 116 (2016) 171101; Phys. Rev. Lett. 117 (2016) 089902 (Erratum), arXiv:1602.07309.
[6] E. Berti, et al., Class. Quantum Gravity 32 (2015) 243001, arXiv:1501.07274.
[7] L. Blanchet, Living Rev. Relativ. 17 (2014) 2, arXiv:1310.1528.
[8] U. Sperhake, E. Berti, V. Cardoso, C. R. Phys. 14 (2013) 306, arXiv:1107.2819.
[9] E. Berti, V. Cardoso, A.O. Starinets, Class. Quantum Gravity 26 (2009) 163001, arXiv:0905.2975.
[10] V. Cardoso, P. Pani, Nat. Astron. 1 (2017) 586, arXiv:1709.01525.
[11] J. Abedi, H. Dykaar, N. Afshordi, Phys. Rev. D 96 (2017) 082004, arXiv:1612.00266.
[12] G. Ashton, O. Birnholtz, M. Cabero, C. Capano, T. Dent, B. Krishnan, G.D. Meadors, A.B. Nielsen, A. Nitz, J. Westerweck, arXiv:1612.05625, 2016.
[13] S. Xin, B. Chen, R.K.L. Lo, L. Sun, W.-B. Han, X. Zhong, M. Srivastava, S. Ma, Q. Wang, Y. Chen, Phys. Rev. D 104 (2021) 104005, arXiv:2105.12313.
[14] J. Westerweck, A. Nielsen, O. Fischer-Birnholtz, M. Cabero, C. Capano, T. Dent, B. Krishnan, G. Meadors, A.H. Nitz, Phys. Rev. D 97 (2018) 124037, arXiv:1712.09966.
[15] A.B. Nielsen, C.D. Capano, O. Birnholtz, J. Westerweck, Phys. Rev. D 99 (2019) 104012, arXiv:1811.04904.
[16] A. Maselli, S.H. Völkel, K.D. Kokkotas, Phys. Rev. D 96 (2017) 064045, arXiv:1708.02217.
[17] K.W. Tsang, M. Rollier, A. Ghosh, A. Samajdar, M. Agathos, K. Chatziioannou, V. Cardoso, G. Khanna, C. Van Den Broeck, Phys. Rev. D 98 (2018) 024023, arXiv:1804.04877.
[18] R.K.L. Lo, T.G.F. Li, A.J. Weinstein, Phys. Rev. D 99 (2019) 084052, arXiv:1811.07431.
[19] K.W. Tsang, A. Ghosh, A. Samajdar, K. Chatziioannou, S. Mastrogiovanni, M. Agathos, C. Van Den Broeck, Phys. Rev. D 101 (2020) 064012, arXiv:1906.11168.
[20] R. Abbott, et al., LIGO Scientific, Virgo, Phys. Rev. D 103 (2021) 122002, arXiv:2010.14529.
[21] V. Cardoso, S. Hopper, C.F.B. Macedo, C. Palenzuela, P. Pani, Phys. Rev. D 94 (2016) 084031, arXiv:1608.08637.
[22] P. Bueno, P.A. Cano, F. Goelen, T. Hertog, B. Vercnocke, Phys. Rev. D 97 (2018) 024040, arXiv:1711.00391.
[23] K.A. Bronnikov, R.A. Konoplya, Phys. Rev. D 101 (2020) 064004, arXiv:1912.05315.
[24] H. Liu, P. Liu, Y. Liu, B. Wang, J.-P. Wu, Phys. Rev. D 103 (2021) 024006, arXiv:2007.09078.
[25] M.-Y. Ou, M.-Y. Lai, H. Huang, Eur. Phys. J. C 82 (2022) 452, arXiv:2111.13890.
[26] W.-L. Qian, Q. Pan, R.G. Daghigh, B. Wang, R.-H. Yue, arXiv:2402.05485, 2024.
[27] R.A. Konoplya, Z. Stuchlík, A. Zhidenko, Phys. Rev. D 99 (2019) 024007, arXiv:1810.01295.
[28] D. Kartini, A. Sulaksono, J. Phys. Conf. Ser. 1572 (2020) 012034.
[29] R. Dey, S. Chakraborty, N. Afshordi, Phys. Rev. D 101 (2020) 104014, arXiv:2001.01301.
[30] A. Chowdhury, N. Banerjee, Phys. Rev. D 102 (2020) 124051, arXiv:2006.16522.
[31] Q. Wang, N. Oshita, N. Afshordi, Phys. Rev. D 101 (2020) 024031, arXiv:1905.00446.
[32] K. Saraswat, N. Afshordi, J. High Energy Phys. 04 (2020) 136, arXiv:1906.02653.
[33] N. Oshita, D. Tsuna, N. Afshordi, Phys. Rev. D 102 (2020) 024045, arXiv:2001.11642.
[34] S.K. Manikandan, K. Rajeev, Phys. Rev. D 105 (2022) 064024, arXiv:2112.08773.
[35] H. Liu, W.-L. Qian, Y. Liu, J.-P. Wu, B. Wang, R.-H. Yue, Phys. Rev. D 104 (2021) 044012, arXiv:2104.11912.
[36] G. D'Amico, N. Kaloper, Phys. Rev. D 102 (2020) 044001, arXiv:1912.05584.
[37] H. Huang, M.-Y. Ou, M.-Y. Lai, H. Lu, Phys. Rev. D 105 (2022) 104049, arXiv:2112.14780.
[38] A. Sang, M. Zhang, S.-W. Wei, J. Jiang, Eur. Phys. J. C 83 (2023) 291, arXiv:2209.02559.
[39] J. Ovalle, R. Casadio, E. Contreras, A. Sotomayor, Phys. Dark Universe 31 (2021) 100744, arXiv:2006.06735.
[40] E. Contreras, J. Ovalle, R. Casadio, Phys. Rev. D 103 (2021) 044020, arXiv:2101.08569.
[41] S. Mahapatra, I. Banerjee, Phys. Dark Universe 39 (2023) 101172, arXiv:2208.05796.
[42] R.T. Cavalcanti, R.C. de Paiva, R. da Rocha, Eur. Phys. J. Plus 137 (2022) 1185, arXiv:2203.08740.
[43] Y. Yang, D. Liu, A. Övgün, Z.-W. Long, Z. Xu, Phys. Rev. D 107 (2023) 064042, arXiv:2203.11551.
[44] Z. Li, Phys. Lett. B 841 (2023) 137902, arXiv:2212.08112.
[45] S.U. Islam, S.G. Ghosh, Phys. Rev. D 103 (2021) 124052, arXiv:2102.08289.
[46] M. Afrin, R. Kumar, S.G. Ghosh, Mon. Not. R. Astron. Soc. 504 (2021) 5927, arXiv:2103.11417.
[47] Y. Meng, X.-M. Kuang, X.-J. Wang, B. Wang, J.-P. Wu, Phys. Rev. D 108 (2023) 064013, arXiv:2306.10459.
[48] Y. Meng, X.-M. Kuang, X.-J. Wang, B. Wang, J.-P. Wu, Eur. Phys. J. C 84 (2024) 305, arXiv:2401.05634.
[49] M.-H. Wu, H. Guo, X.-M. Kuang, Phys. Rev. D 107 (2023) 064033, arXiv:2306.10467.
[50] C. Liu, H. Siew, T. Zhu, Q. Wu, Y. Zhao, H. Xu, arXiv:2311.12423, 2023.
[51] T. Zi, P.-C. Li, Phys. Rev. D 108 (2023) 084001, arXiv:2306.02683.

[52] G. Guo, Y. Lu, P. Wang, H. Wu, H. Yang, Phys. Rev. D 107 (2023) 124037, arXiv:2212.12901.
[53] V. Cardoso, A.S. Miranda, E. Berti, H. Witek, V.T. Zanchin, Phys. Rev. D 79 (2009) 064016, arXiv:0812.1806.
[54] R. Ruffini, J.A. Wheeler, Phys. Today 24 (1971) 30.
[55] J. Ovalle, Phys. Rev. D 95 (2017) 104019, arXiv:1704.05899.
[56] E. Abdalla, C.E. Pellicer, J. de Oliveira, A.B. Pavan, Phys. Rev. D 82 (2010) 124033, arXiv:1010.2806.